# Calculation of GIC in the North Island of New Zealand using MT data and thin-sheet modelling

**K. Mukhtar[1], M. Ingham[1], C. J. Rodger[2], D. H. Mac Manus[2], T. Divett[2], W. Heise[3], E. Bertrand[3], M. Dalzell[4] and T. Petersen[3]**

[1]School of Chemical and Physical Sciences, Victoria University of Wellington, Wellington, New Zealand
[2]Department of Physics, University of Otago, Dunedin, New Zealand
[3]GNS Science, Lower Hutt, New Zealand
[4]Transpower New Zealand Limited, New Zealand

Corresponding author: Malcolm Ingham (malcolm.ingham@vuw.ac.nz)

## Key Points:

- GIC in the North Island of New Zealand were modelled for the St. Patrick's Day 2015 storm and the storm of 20 November 2003
- Calculations based on MT data and thin-sheet modelling were compared
- Substations and individual transformers that may be at risk during significant space weather events were identified

## Abstract

Geomagnetically induced currents in the North Island New Zealand power transmission network during two large magnetic storms are calculated from both magnetotelluric (MT) data and a thin-sheet conductance model of New Zealand previously used to study GIC in the South Island. We focus on the 2015 St. Patrick's Day magnetic storm and the storm of 20 November 2003. Lack of MT data in the north-western part of the Island means that the transmission network in this region is represented by an equivalent circuit. Lack of GIC observations in the North Island means that results cannot be directly compared with measured GIC. However, our calculation of GIC shows that substations and individual transformers in the lower part of the Island with significant currents are generally the same as those where total harmonic distortion has been observed during periods of enhanced geomagnetic activity. MT data in the period range 2-30 minutes are used to predict GIC associated with the sudden storm commencement and rapid variations in the magnetic field. In contrast, the thin-sheet modelling approach shows that GIC may be expected to occur in conjunction with longer period variations. Calculations for the 2003 storm suggest that at some locations GIC in excess of 10 A may persist for long periods of time and may produce significant harmonic distortion which could lead to localized transformer heating. It is concluded that despite its relatively low latitude the North Island power network is potentially at risk from significant GIC during extreme storms.



## Plain Language Summary

Variations in the Earth's magnetic field with time during so-called "magnetic storms" can result in currents (geomagnetically induced currents – GIC) entering and leaving power transmission lines through the ground connections on transformers. Large GIC, or even smaller currents occurring repeatedly, can not only damage transformers but, in the worst case scenario, cause disruption to an entire transmission network. To attempt to assess the potential vulnerability of the transmission network in the North Island of New Zealand to such effects, we present model calculations of GIC resulting from two magnetic storms. The results show that despite the relatively low geomagnetic latitude of New Zealand's North Island there are some substations and individual transformers where large GIC can be expected and may be problematic.


## 1 Introduction

Geomagnetically induced currents (GIC) can present a serious risk to power networks during significant geomagnetic storms (United Nations, 2017). Although the electric field induced in the ground by the time varying magnetic field is generally only of the order of mV/km, during extreme storms local fields can be as large as 1 V/km such that long transmission lines can have significant potential differences driving quasi-dc currents. Entering and leaving transmission lines through the neutral connections on transformers, GIC can lead to both overheating in those transformers (Kappenman, 1996) and the generation of harmonics due to half cycle saturation in the transformer core (Girgis & Vedante, 2015). In the most serious cases this could result in severe disruption of an entire transmission network.

GIC have been modelled using a variety of techniques and in many countries. The main requirement of such studies is to estimate the spatial and temporal variation in the induced electric field during a geomagnetic storm. Integration of the electric field over the known geometry of a transmission network, with knowledge of the line and grounding resistances allows calculation of the resulting GIC through, for example, the widely used matrix method of Lehtinen and Pirjola (1985). To calculate electric fields many studies have employed the numerical thin-sheet modelling technique of Vasseur and Weidelt (1977) in which spatial variations in the ground electrical conductivity are embodied in a two-dimensional thin sheet with laterally varying conductance. Such models have been used by Mackay (2003) and Beggan et al. (2013) to study GIC in the United Kingdom; by Kelly et al. (2017) and Bailey et al. (2017, 2018) in continental Europe; and Divett et al. (2017, 2018, 2020) in New Zealand. Although such models are generally based on field measurements of electrical conductivity structure measured using magnetotelluric sounding (MT), they tend to give a simplified picture of lateral variations. There are also numerical restrictions on the range of frequencies of variation which can be modelled, as well as on the discretization of the conductance (Divett et al., 2017). As an alternative the MT impedance tensor can be used directly to estimate electric fields in the frequency domain from geomagnetic field spectra, as has been done by Blake et al. (2016) to calculate GIC in the Irish power network; by Torta et al. (2017) in Spain, and extensively by Bonner & Schulz (2017), Kelbert et al. (2017), Love et al. (2018) and Lucas et al. (2018) in the United States. In principle the use of the MT impedance tensor allows a much broader range of frequencies to be explored than is possible using the thin-sheet model and also allows incorporation of much finer detail than the thin sheet modelling approach.

Thus far, modelling studies on GIC in New Zealand (Figure 1) have concentrated on the South Island. Lying between latitudes of 41 and 47 °S, and in relative proximity to the auroral zone, the South Island has traditionally been presumed to be at higher risk from GIC than the North Island which lies at latitudes between 34 and 42 °S. Furthermore, the South Island transmission network has an extensive archive of GIC measurements, acquired by Transpower New Zealand Ltd., the network operator, at many substations and individual tranformers (Mac Manus et al. 2017; Rodger et al. 2017). The North and South Island power networks are isolated with the only connection between the Islands being through a High Voltage DC (HVDC) link which prevents the flow of GIC between them (more information on the New Zealand HVDC link and the New Zealand DC measurements can be found in Mac Manus et al. (2017)). Direct measurements of GIC in the North Island exist only near Wellington close to the northern termination of the HVDC link.

Despite this there is evidence for GIC-impacts in the North Island. Measurements of total harmonic distortion (THD) are made at over 120 locations in the New Zealand transmission network including many in the North Island. Saturation of a transformer core resulting from GIC can lead to the generation of voltage harmonics in the power system (Girgis & Vedante, 2015). Clilverd et al. (2017) have demonstrated the occurrence of this at HWB substation near Dunedin in New Zealand's South Island. Analysis by Rodger et al. (2020) of THD measurements associated with geomagnetic activity between 6-9 September 2017 shows significant THD occured at several locations in the North Island during the storm peaks, suggesting the existence of previously undetected GIC in the North Island power network. Many of these locations are close to New Plymouth in Taranaki in the western part of the North Island (marked in Figure 1).

Due to the relative paucity of MT measurements in the South Island, studies of South Island GIC have used the thin-sheet modelling technique. In this paper we assess the potential risk posed to the North Island power transmission network using both the thin-sheet approach and using extensive MT measurements, made in the North Island over many years, to calculate GIC resulting from two separate magnetic storms. The storms used are the St. Patrick's Day storm of 2015 and the storm of 20 November 2003. For both storms we use magnetic field variations observed at the INTERMAGNET geomagnetic observatory Eyrewell (EYR) near Christchurch. The use of the field variations for these storms gives a useful indication of the likely magnitude of GIC occurring in the North Island during relatively significant, but not extreme, geomagnetic events (Rodger et al., 2017). We begin with a discussion of the two storms and outline the way in which we use the magnetic field measurements to calculate time varying electric fields using both the MT data and the thin-sheet model. In doing this we include a brief review of the thin-sheet model of New Zealand as used by Divett et al. (2017, 2018, 2020) and of this model's limitations. We then discuss the available MT data. As the MT data does not cover the entire extent of the North Island, we discuss the interpolation and extrapolation of calculated electric fields to cover gaps where no MT data exist. This demonstrates that lack of MT data in the northern part of the North Island means that realistic electric fields cannot be estimated for that region. As a result, we present and justify the use of an equivalent circuit to represent this northern part of the transmission network. This follows the suggestions of Boteler et al. (2013) whereby a network adjacent to that under study can be represented by suitable Thevenin equivalent voltages and resistances. The GIC predicted for each storm for the remainder of the North Island network are then presented. Although the GIC predicted from the MT data due to short period variations in the magnetic field appear to be reasonable, the longest period to which the MT data extend is about 30 minutes. Thus, GIC resulting from longer period variations are not captured. We demonstrate that at these longer periods GIC may be better predicted by the thin-sheet model. We finally compare calculated GIC with both GIC observed during the storm at a suitable location in the South Island, and with the THD results of Rodger et al. (2020).

## 2 The magnetic storms of St. Patrick's Day 2015 and 20 November 2003

As noted above the two magnetic storms for which GIC have been calculated are the St. Patrick's Day storm of 17 March 2015 and one of a series of storms which occurred in late November 2003. The St. Patrick's Day storm was the largest geomagnetic storm of solar cycle 24 (Navia et al. 2018), with a minimum Dst value of -222 nT and a Kp-index which reached 8- for a period of about 12 hours. In a New Zealand context and considering the rate of change of the horizontal magnetic field, this was the 13th largest storm in the 15 year period from the start of 2001 to the end of 2015 (Rodger et al., 2017). The variations in the horizontal magnetic field components measured at the Eyrewell (EYR) geomagnetic observatory near Christchurch in New Zealand's South Island during the St. Patrick's Day storm are shown in Figure 2(a). The time series spans approximately 1.5 days starting from 0000 (UT) 17 March 2015 and for data processing purposes 2048 data points have been selected with a 1-minute sampling interval. The data span encompasses both the main storm and recovery phases.

The magnetic storm of 20 November 2003 was one of a series of large magnetic storms during the months of October and November 2003. It recorded the lowest value of Dst index of all of these storms of -490 nT during the main phase of the storm, almost reaching the -500 nT threshold below which storms are categorized as super magnetic storms (Lakhina & Tsurutani, 2016) . The Kp-index also stayed at its maximum value of 9 for a period of 6 hours. (15-21 UT). In the same New Zealand context mentioned above, this was the 10th largest storm in the 15 years from 2001 to 2015. The horizontal magnetic field variations at EYR during this storm are shown in Figure 2(b).

It has been assumed in the modelling which follows that these magnetic field variations are spatially uniform across the North Island of New Zealand. The validity of this assumption has recently been tested by Divett et al. (2020) for the South Island and found to give only minor differences in geoelectric fields calculated using the thin-sheet approach compared to a spatially varying field.

## 3 Calculating electric fields

### 3.1. Calculation of electric fields from MT data

To calculate the resulting electric fields at an MT site produced by the magnetic field variations during each storm the following procedure has been adopted. (1) A Fast Fourier Transform (FFT) has been applied to transform the horizontal magnetic field variations into the frequency domain. (2) Each spectral component of the magnetic field variation has then been used to calculate the corresponding spectral component in the induced horizontal electric fields using the magnetotelluric impedance tensor $\underline{\underline{Z}}$

$$\begin{aligned} E_x &= Z_{xx}B_x + Z_{xy}B_y \\ E_y &= Z_{yx}B_x + Z_{yy}B_y \end{aligned} \qquad (1)$$

in which the units of the tensor elements $\begin{pmatrix} Z_{xx} & Z_{xy} \\ Z_{yx} & Z_{yy} \end{pmatrix}$ are such that expressing $B_x$ and $B_y$ in nT gives $E_x$ and $E_y$ in mV/km. (3) Although in general measurements at MT sites have been made in the frequency range 300-0.0005 Hz, given the 1 minute sampling of the magnetic field only discrete periods between 1 and approximately 30 minutes have been used in the calculation of electric fields. Simple polynomials have been fitted to the real and imaginary parts of each impedance tensor element to allow values to be interpolated to all periods in the magnetic field spectra that lie in this range. Magnetic field variations outside this range are ignored. (4) The frequency domain geoelectric fields so calculated are then transformed into the time domain by applying an Inverse Fast Fourier Transform (IFFT). An example of electric fields at a single MT site (MTR106, measured as part of the MT survey of Mount Ruapehu reported by Ingham et al.,2009) calculated in this manner for the St. Patrick’s Day storm is shown in Figure 3 and clearly shows the large electric fields generated during the sudden storm commencement (SSC) which for this storm began at 04:45.

### 3.2. Calculating electric fields from the thin-sheet model

To calculate time varying electric fields from the thin-sheet model, a similar procedure has been used. The amplitude and phase of the $B_x$ and $B_y$ magnetic field spectra for a storm, for each period given by FFT, have been used to calculate the resulting electric fields in each cell of the model at that period. The electric field spectra so generated have been turned into time series using an IFFT. As Figure 2 represents a 2048 minute time series with 1 minute sampling for each storm, the period range of variations covered by the electric fields calculated from the thin-sheet model is from 2-2048 minutes.

The thin-sheet modelling technique of Vasseur & Weidelt (1977) was originally formulated to model the distortion by lateral variations in conductivity of currents induced in the Earth. The validity of the technique of representing 3-dimensional conductive structure through 2-dimensional variations in the conductance of a thin-sheet at the surface has several numerical restrictions. In these, quantities are generally expressed in terms of the skin-depth ($\delta$) of variations in the layered structure which underlies the thin-sheet. Using this nomenclature the two principal conditions for validity are

$$h \ll 1 \qquad (2)$$

$$\left(\frac{h}{\eta}\right)^2 \ll 1 \qquad (3)$$

where $h$ is the thickness of the thin-sheet, that is the depth range over which the conductance has been calculated, and $\eta$ is the skin depth in the thin-sheet. A third condition relates to the spacing of the numerical grid, which must be less than $\delta/4$. It is in satisfying equation (3) above that thin-sheet model is most limited with regard to the North Island.

That part of the thin-sheet model used by Divett et al. (2017) containing the North Island of New Zealand is shown in Figure 4. For a period of variation of 10 minutes, for a skin depth $\delta$ of about 190 km in the underlying layered structure, the value of $h/\delta$ is 0.105, which satisfies equation (2). In the highly conductive regions, with conductance 500 S, $(h/\eta)^2$ is 0.069, satisfying equation (3). For the shortest periods of variation relevant to GIC studies, ~2 minutes, the respective values are 0.235 and 0.346, arguably marginal in satisfying these conditions. However, even in the shallow coastal seas adjacent to the land the integrated conductance in the thin-sheet is 3000 S (pale blue in Figure 4) meaning that at 2 minutes period $(h/\eta)^2$ is in fact greater than unity. Indeed, even neglecting the much higher conductance values representing the deeper ocean, equation (3) can only really be said to be met for periods greater than about 10 minutes. This failure to meet the validity conditions at short period means that for these periods GIC calculation based on the thin-sheet electric fields must be treated with caution.

## 4 The North Island power transmission network

The transmission network in the North Island of New Zealand is shown in Figure 5. The North Island transmission network principally consists of transmission lines with voltage ranges of 110 kV and 220 kV. However, a 400 kV line connects Whakamaru (WKM), to the north of Lake Taupo, with Auckland. Within the North Island the majority of power is generated at a series of hydroelectric stations along the Waikato River which flows from Lake Taupo in the centre of the Island through Hamilton (HAM) reaching the west coast to the south of Auckland. Other power stations based on geothermal, coal, gas and wind are spread around the Island. The HVDC link which brings power from the major hydro lakes in the South Island terminates at Haywards (HAY) just to the north of Wellington. In total there are 33 power stations and 84 separate substations. As discussed for the South Island by Divett et al. (2017), for substation GIC calculation the North Island network has been represented using the approach of Lehtinen & Pirjola (1985). Thus, power station/substation nodes are connected by line resistors and earthed through earth ground resistors using line and grounding resistance values provided by Transpower New Zealand Ltd. Similarly, the extension to calculate GIC at transformer level follows the method given by Divett et al. (2018) and is based on describing autotransformers and normal transformers in the manner described by Boteler & Pirjola (2014).

## 5 Magnetotelluric data and extrapolation/interpolation of electric fields

### 5.1. Data distribution

A large number of magnetotelluric studies have been conducted in the North Island of New Zealand. These include studies by Bertrand et al. (2012, 2013), Heise et al. (2008, 2010, 2014) and Ingham (2005) in the Central Volcanic Region, by Cassidy et al. (2009), Ingham et al. (2009) and Stagpoole et al. (2009) on the volcanic systems, and by Heise et al. (2012), Ingham et al. (2001) and McLoughlin et al. (2002) along the east coast of the Island. In total well over 200 separate MT measurements have been made. Of these sites many are in very close geographic proximity but, overall, sites have been measured in 115 of the 463 20 km x

20 km cells which make up the North Island in the thin-sheet conductance model used by Divett et al. (2017). The distribution of these 115 sites is shown as black dots in Figure 4.

The conductance map of North Island shows five main regions. The east coast is dominated by high conductance associated with the Hikurangi subduction margin, and a dense array of MT data exists in this region. Low conductance immediately to the west of that region is associated with the mountainous spine of the North Island where resistive greywacke outcrops. There are few measurements in this region (shown in light green in Figure 4). A dense array of MT sites exists in the centre of the Island where high conductance values are associated with the Central Volcanic Region, and a small number of sites are distributed along the west coast from the Wellington to New Plymouth. However, through much of the west and north-west of the Island MT data are either scarce or absent; because of this the conductance shown in Figure 4 has been estimated purely from knowledge of the geology. It is the lack of MT data in this region that subsequently, as described below, leads to the use of an equivalent circuit to represent the northern part of the transmission network.

5.2. Calculation and interpolation/extrapolation of electric fields

As is apparent from Figure 4, the 115 MT sites are largely distributed in the southern and eastern parts of the North Island. In particular, the northern part of North Island is completely devoid of any MT data. There are also gaps in the distribution of sites both down the relatively resistive mountain belt and in the western part of the lower North Island. Calculation of GIC from the distribution of transmission lines in the North Island (Figure 5) requires, at a minimum, values for the geoelectric fields in each cell of the model domain where substations are located and also those that power lines pass through. To fill the gaps in the mountain regions and in the lower North Island electric fields calculated for surrounding sites can be interpolated, whereas extrapolation is necessary to give fields in the region extending to the north.

Mathematically there are several different interpolation techniques for 2-D scattered data. These include nearest neighbour (or proximal) interpolation, bilinear interpolation, and biharmonic spline interpolation. The simplest of these is the nearest neighbour technique which assigns the electric field in the nearest cell for which measurement exists to an empty cell. Bilinear interpolation is based on interpolation using the four nearest values of electric field, while biharmonic spline interpolation is based on cubic interpolation in two-dimensions of the values at the nearest cells. After first calculating the time variations in $E_x$ and $E_y$ at each MT site in the manner described above these interpolation techniques have been tested for two different time instances during the St. Patrick's Day Storm. The results of this, represented as the electric field vectors in each cell, are shown in Figure 6 for nearest neighbour interpolation and biharmonic spline interpolation.

At both 04:46 UT, immediately after the sudden storm commencement, and at 09:04 UT, just as $B_x$ and $B_y$ start to increase and decrease by 100 nT respectively, but more gradually (Figure 2), Figure 6 shows both interpolation techniques are effective in the eastern and lower parts of the North Island where MT sites are well distributed. The two interpolation techniques also give field magnitudes and directions in agreement with each other in these parts of the North Island. However, to the north of a south-west to north-east line roughly to the south of Hamilton (marked in Figure 1, and as the substation HAM in Figure 5), where there are no MT sites and the fields are extrapolated, the calculated electric field vectors are clearly unrealistic. These unrealistic northern field vectors are particularly true for the region to the north of Auckland where the two interpolation techniques yield electric fields which differ significantly in orientation. The extrapolated fields generated by the biharmonic splines also have unrealistically large magnitude. As such the use of such extrapolated geoelectric fields in the calculation of GICs in the transmission network is likely to lead to significant errors. To avoid this the approach of using an equivalent circuit to represent that part of the network north of the dashed line in Figure 5 has been investigated. To the south of this line the interpolated/extrapolated electric fields are judged to be reliable.

## 6 Using an equivalent circuit to represent the northern part of the network

To avoid the impact of unrealistic extrapolated electric fields on the calculation of GIC, an equivalent circuit approach has been explored to cover the area where there is no MT data. Although this approach will not result in the calculation of GICs for the whole of the North Island power network, the lower part of the network may be able to be realistically modelled using this technique. Boteler et al. (2013) discussed different equivalent circuit approaches to modelling the effect of a neighbouring network. These involve the use of Thevenin equivalent voltage and resistance values for the part of a network being represented in this way. For example, the simplest approach is to completely ignore the neighbouring network (in this case the northern part of the North Island) and leave the connection as an open circuit. In this case the equivalent (Thevenin) circuit voltage and resistance would be $V_{th} = 0$ and $R_{th} = \infty$. This approach incorporates no information from the neighbouring network. In contrast, Boteler et al. concluded that the most appropriate equivalent circuit approach uses the line voltage connecting the two neighbouring networks and the line resistance i.e. $V_{th} = V_L$ and $R_{th} = R_L$.

To implement this approach we have disconnected the part of network where there is no MT data - the area to the north west of the black dashed line shown in Figure 5. There are, however, a few long power lines which originate from substations south of this line, locations which have been labelled in Figure 5. The power lines in question, from Arapuni (ARI), Whakamaru (WKM), Taumarunui (TMN) and Stratford (SFD), extend towards the north where extrapolated geoelectric fields have been calculated. The line lengths, resistances and connection points of these lines are given in Table 1. For the purposes of GIC calculation the northern ends of these lines (i.e. at the substation listed in column 3) have been earthed. The importance of including these lines is that they connect the parts of the network to the north and south of the black dashed line in Figure 5 and, having, long lengths, may have a significant effect on the lower part of network.

To check the validity of this approach we have calculated GIC resulting from hypothetical uniform geoelectric fields of different orientations. Geoelectric fields of 1 V/m in different orientations in intervals of 45 degrees are applied to whole of the North Island and the resulting GIC computed. The same electric fields are then applied with the northern part of the network disconnected, as outlined above, and with the lines listed in Table 1 earthed at their northern ends. The resulting calculated substation GICs, for the part of the network south of Huntly (HLY) are shown in Figure 7. Disconnecting the northern part of the network and grounding the lines listed in Table 1 clearly has minimal effect on the calculation of GICs in the lower part of the network. The calculated GICs are very nearly the same for all substations, with only small differences at substations connected through the transmission lines listed above.

Although the magnitude of electric field used in the calculations is much larger than would be expected to occur during a typical large geomagnetic storm, it is interesting to examine how the magnitude of GIC at some substations changes with the orientation of the field. In the lowermost part of the North Island (e.g. Haywards (HAY) and Bunnythorpe (BPE)) large GIC are observed to result when the electric field has a northward component.

North and north-west oriented fields also result in large GIC at Redclyffe (RDF) on the east coast. Such observations can presumably be correlated with the orientation of the main transmission lines to and from these substations in that when power lines and electric fields are in parallel more current is drawn into the network than when they are in perpendicular directions. Large GIC at New Plymouth (NPL), however, occur for north, north-east and east oriented geoelectric fields while the main lines into this station run north-west. Further to the north the largest GIC occur at Kawerau (KAW). Calculations using the uniform field for the entire network also show significant GIC at some of the substations replaced by the equivalent circuit. These include HLY, Otahuhu (OTA) and Penrose (PEN), with the overall sum of GIC into and out of the network of necessity being zero.

## 7 Results

### 7.1. North Island GIC calculated from MT electric fields

Having justified the use of an equivalent circuit to represent the northern part of the North Island transmission network the electric fields calculated at each minute interval of the both the 2015 St. Patrick’s Day Storm and the 2003 storm have been interpolated, as described above, and use to calculate the time variation of GIC at both substation and transformer-level in that part of the network south of the dashed line in Figure 5. The importance of modelling GIC at the transformer-level has been outlined by Divett et al. (2018). A principal reason is that it is individual transformers that are most likely impacted by space weather events and, in the same substation, not all transformers are necessarily affected similarly as grounding resistances and internal connections may differ. Equally, although measurements of GIC in the North Island are not available, such measurements are normally made on individual transformers rather than at a substation level. Divett et al. (2018) also explained how such transformer level modelling follows from the work of Boteler & Pirjola (2014, 2017).

The substation-level GIC calculated for New Plymouth (NPL) for both storms are shown in Figure 8. For the St. Patrick’s Day storm the largest GIC calculated using the MT data and the equivalent circuit are associated with the SSC. The GIC goes from greater than 9 A in one direction to over 13 A in the opposite direction over 1 minute. Inspection of the orientation of the electric fields shows that this reversal reflects a general change in the direction of the electric field from north-east to south-west. This itself is in response to rates of change of the horizontal magnetic field, as measured in the 1-minute resolution magnetometer data from the EYR observatory, of an increase of just less than 70 nT/min followed by a decrease of about 20 nT/min. A similar, but slightly less dramatic change in GIC, occurs at the nearby Stratford (SFD) substation, while on the east coast a change from 1 A to −9 A takes place at RDF as well as at nearby Whirinaki (WHI). Further south, large negative GIC occur at BPE and Haywards (HAY). To the north the most significant GIC associated with the SSC of the St. Patrick’s Day storm is at Kawerau (KAW). Figure 8 also shows that relatively large oscillations in GIC also occur during the main phase of the storm with a period of between 6 and 8 minutes and maximum rates of change of ~15 nT/min.

In contrast, during the much larger storm of 20 November 2003 the maximum rates of change of the horizontal magnetic field given by the 1-minute resolution data from EYR occurred not during the SSC but much later during the main phase of the storm. Between about 1745 and 1945 UT rates of change of ±40 nT/min in the northward component of the magnetic field were frequent with peak values of around +60 nT/min and -70 nT/min. Simultaneous rates of change in the eastward component were about half of these values. The effect of these peak rates of change is seen in the lower panel of Figure 8. The peak GIC at NPL of over 40A occurs during the mail phase of the storm and there is no significant GIC associated with the SSC. Figure 9 shows GIC calculated in other substations in the lower North Island at 18:48 UT on 20 November 2003 calculated using the MT data. GIC of near or over 20 A are seen at BPE, and also at Haywards (HAY) just to the north of Wellington. Overall, during the whole period of the 2003 storm, 15 substations in that part of the North Island for which GIC are calculated experience peak GIC of over 5 A. Of these in addition to NPL, BPE and HAY, another 5 substations (RDF, WHI, SFD, WRK and KAW) have peak GIC in excess of 10 A.

The difference in peak GIC between the two storms, for example at NPL, when the maximum rates of change of the horizontal magnetic field are similar is somewhat surprising. It may partly be explained by the duration of the field changes. During the 2003 storm, around the time of the peak GIC and peak rate of change of the field, the horizontal field actually increased continuously by over 500 nT over a period of 20 minutes. Such a sustained rate of change did not occur during the SSC of the 2015 St. Patrick's Day storm, when the peak GIC was calculated.

The transformer-level response as calculated from the MT data is very similar to the substation response. For the St. Patrick's Day storm, the largest ranges of GIC are observed during the SSC at the only transformer at NPL, NPL T8 (-9.3 A to 13.1 A), SFD T10 (-6.5 A to 11.5 A) and RDF T1 (-9.8 A to 4.4 A). However, at WHI where large substation-level GIC are observed, at transformer-level these are divided almost equally between 6 separate transformers. A similar division of GIC between transformers is observed at RDF where GIC in transformer T3 and T4 are generally half or less than, those in transformer T1, and a fourth transformer, T2, shows practically no GIC. This emphasizes the importance placed on this level of calculation by Divett et al. (2018) in understanding which individual transformers at a given substation are at risk from GIC.

### 7.2. Comparison with GIC calculated from the thin-sheet model

Also shown in Figure 8, by red lines, are the GIC predicted by the electric fields calculated from the thin-sheet model of Divett et al. (2017). In this case, for the purposes of direct comparison, the calculated GIC have been band-pass filtered to match the period range of the MT data (2-30 minutes). Whereas significant GIC are observed from the MT/equivalent-circuit calculation, this is not generally the case for the electric fields calculated from the thin-sheet model. For example, during the SSC of the 2015 St. Patrick's Day storm the calculated GIC at NPL changes only from -1.8 A to 2.5 A, with similarly small changes at the other substations. The subsequent lower frequency GIC match those from the MT/equivalent circuit calculation much better both in terms of phase and amplitude. This is true also for the longer period GIC calculated for the 2003 storm. This difference between the GIC produced by the SSC and by lower frequency variations may reflect the numerical constraints that exist for the thin-sheet model at high frequency/short period.

Not shown in Figure 8, and not reproduced by the MT electric field calculation due to the restricted bandwidth of the data, are much longer period GIC variations (at periods between 30 and 2048 minutes) which are evident in the calculations based on thin-sheet electric fields. The unfiltered substation-level GIC response at NPL calculated from the thin-sheet model for the St. Patrick's Day storm is shown in Figure 10. Also shown is the variation in the northward component of the magnetic field ($B_x$) at EYR during the storm. It is evident that the thin-sheet calculation suggests that GIC do occur in response to these longer period variations in the magnetic field during the main and recovery phases of the storm. Although the GIC resulting from the SSC may be significantly underestimated by the thin-sheet calculation due to the numerical constraints, it seems likely that longer period GIC may be better captured by this calculation than by one based on the period limited MT data. These longer period GIC at NPL calculated from the thin-sheet model and shown in Figure 10 range between extrema of +5 A and -5 A and may be additionally important in terms of the impact upon a transformer.

Closer inspection of the GIC timeseries for both the MT and thin-sheet calculations indicates that, as suggested above, peak GIC may not only be larger than the figures quoted but may also, in individual transformers, persist for longer. Shown in the lower part of Figure 8 are the GIC in transformer T8 at NPL calculated from both the MT data (black line) and the thin-sheet model (red line) for a 12 hour period during the 20 November 2003 storm. As for the St. Patrick's Day storm the GIC calculated from the thin-sheet model have been band-pass filtered to match the period range of the MT data. The temporal match between the GIC from the two calculations is excellent but, as indicated above, the GIC calculated from the thin-sheet model are smaller than those calculated from the MT measurements. Figure 11(a) shows a closer look at the MT calculated GIC over 2 hours from 1730-1930 UT when the GIC swing from positive to negative with a dominant periodicity of about 15-20 minutes. Over this 2 hour time span the magnitude of the GIC exceeds 10 A for a total time of 43 minutes. This includes 5 periods during which the GIC remains above 10 A continually for 5 minutes. Similar numbers are applicable to other individual transformers, for example RDF T1. The persistence of large, but not peak value, GIC for a continuous length of time potentially present a significant risk to a transformer from localized heating, and the surrounding network from harmonic distortion.

In reality the situation is probably worse. Figure 11(b) shows the unfiltered GIC in NPL-T8 calculated from the thin-sheet model. As was seen in Figure 10, significantly longer period GIC occur which are not reflected in the period-limited MT data. Thus, even though this is not seen in the thin-sheet GIC in Figure 8, the thin-sheet GIC magnitude is in excess of 10 A for a continuous period of about 45 minutes from 17:25 to 18:10 UT. When such longer period GIC are taken into account it is highly likely that not only will significant GIC persist for much longer time periods but that peak GIC will be even larger than those indicated in Figure 8.

## 8 Validation of GIC predictions

The lack of GIC measurements in the North Island of New Zealand means direct comparison of the GIC calculated from the MT data with observations on individual transformers is not possible. It is possible, however, to ascertain that the calculated GIC do appear to have the appropriate time variations and the correct order of magnitude. To do this we compare the GIC calculated for the St. Patrick's Day storm for Redclyffe (RDF) transformer T1 with those actually observed on transformer T6 at Islington (ISL) near Christchurch in the South Island. Such a comparison can be argued to be meaningful as the physical locations and set-ups of both substations have considerable similarity. RDF and ISL are situated close to the east coast of the North and South Islands respectively. Both are also situated in relatively conductive elongated south-west to north-east regions which are bounded to the north-west by much more resistive terrain associated with the adjacent mountains (Figure 12(b)). A further similarity is in the orientation and lengths of transmission lines connected to the substations. At ISL (Figure 12(a)) lines connect to the substation from both the south-west and the north-east, running essentially parallel to the coast. A single line connects ISL to the west coast of the South Island. This situation is broadly comparable to that seen in Figure 5 for RDF for which, again, lines connect from both the south-west and north-east, with a single line connecting to RDF from the centre of the North Island to the north-west.

Shown in Figure 12(c) are the MT calculated GIC for RDF T1 and the observed GIC for ISL T6, interpolated to 1-minute sampling, around the time of the SSC of the St. Patrick's Day 2015 Storm. The ISL T6 observations have been filtered to match the period range of the MT data. The most noticeable feature is the similarity in the GIC associated with the SSC itself, reaching just over -10 A in both cases. Subsequent GIC are small but show very similar time variations. In general, over the whole period of the storm, GIC at RDF T1 are slightly larger than at ISL but not sufficiently so as to suggest that values are significantly overestimated. This lends some confidence to the assertion that the GIC calculated for the North Island network using the MT data are realistic at least for the period range covered by the impedance tensor.

In terms of GIC occurring over a longer time scale, Rodger et al. (2020) discussed the generation of even harmonics by asymmetric saturation of transformers caused by the quasi-dc nature of GIC. Such harmonic distortion has been implicated in the collapse of the Hydro-Québec transmission network in March 1989 (Guillon et al., 2016) and gives independent evidence of a stressed transformer. Rodger et al. principally looked at even-total harmonic distortion (THD) for transformers in both the North and South Islands during strong geomagnetic activity over 6-9 September 2017. Using observations of GIC magnitude averaged over 10 minutes at locations in the South Island, their general conclusions were that although a SSC may produce significant magnitudes of GIC, these exist for a short enough time duration that they do not result in significant harmonic distortion. In contrast GIC that have a large enough absolute magnitude for an extended period do result in noticeable even-THD.

Rodger et al. also briefly analyzed the degree of even-THD for the St. Patrick's Day storm of 2015, focusing on two periods during which the 10-minute average GIC magnitude at Halfway Bush substation near Dunedin was significant. For the period 0950-1000 UT the most significant even-THD in the North Island was at substations in Hawkes Bay (e.g. Redclyffe) although even-THD was observed relatively widely at low level at many other locations, including substations in Taranaki. Similar, but slightly lower values of even-THD, were observed for the period 1320-1330 UT. The 10-minute averaged GIC calculated at NPL and RDF using the electric fields derived from the MT data for these periods are shown in Table 2.

The small values of the 10-minute averaged GIC are a result of the limited period range covered by the MT data which has the effect of reducing the 10-minute average. Also listed in Table 2 are the unfiltered 10-minute average GIC values given by using the thin-sheet electric fields which contain, as seen in Figure 10, longer period variations in GIC than are shown by the MT data. Particularly for the first of the time windows, these yield values of 10-minute averaged GIC that are significantly higher than those given by the MT data. This supports the implication from analysis of both the St. Patrick's Day and 2003 storms that although the GIC calculated from the MT data may be accurate for GIC produced in response to rapid changes in the magnetic field, they may be underestimates of values during periods where the magnetic field varies significantly over a longer period.

Before considering the overall implications of these results for the hazard presented to the North Island transmission network by space weather events it is worth revisiting the assumption that magnetic field variations across the North Island can be adequately represented by those observed at Eyrewell magnetic observatory. As previously outlined, Divett et al. (2020) found this to be a reasonable assumption for the St. Patrick's Day storm. In analyzing the THD occurring between 6-9 September 2017 Rodger et al. (2020) selected time periods where there were GIC associated with a significant rate of change of the horizontal magnetic field. They calculated such rates using magnetic field observations from 4 separate locations, 2 close to Dunedin, the Eyrewell observatory and at a single location (Te Wharau) in the lower North Island. For a SSC occurring at 2302 UT on 7 September the rates of change of the field were about 10 nT/min at Dunedin dropping to 6.6 nT/min at Te Wharau. Observed GIC and even-THD at 0145 UT on 8 December were associated with rates of change of the horizontal field of 10 nT/min at Dunedin, 5.3 nT/min at EYR and 3.7 nT/min at Te Wharau. A large rate of change of 30.6 nT/min at Dunedin between 1200 and 1300 UT 8 September saw smaller rates of change at EYR (12.3 nT/min) and Te Wharau (7.9 nT/min), while, in accordance with the result of Divett et al. (2020), rates of change during the St. Patrick's Day storm were relatively uniform across all four locations. Additionally, shown in Figure 13 is a comparison of rates of change ($dB_x/dt$) of the northward component of the magnetic field at an MT site close to New Plymouth and at the Eyrewell geomagnetic observatory. These are calculated every minute over a period of 5 hours on 11 November 2019. Although the rates of change are not large during what were essentially relatively quiet magnetic conditions, the largest rates are comparable to those measured at Te Wharau by Rodger et al. during periods where THD was observed. It is evident from Figure 13 that there is a good correlation between $dB_x/dt$ at the two locations. This further supports the suggestion that field variations at Eyrewell do indeed give a reasonable estimate of those in the North Island although how good this comparison is will vary from storm to storm with, on occasion, rates of change of the field in the lower North Island perhaps being only 60-70% of those at EYR.

## 9 Discussion and conclusions

We have presented the first analysis of GIC in New Zealand using electric fields calculated from both magnetotelluric impedance tensor measurements and from a thin-sheet model. This study also represents the first prediction of the likely occurrence of GIC in the North Island transmission network based on analysis of electric fields induced by the time varying magnetic field. We have concentrated on the GIC produced during two magnetic storms: the St. Patrick's Day Storm of 2015 and the storm of 20 November 2003. Coverage of the MT data restricts the analysis to the lower part of the North Island with the upper part being represented by an equivalent circuit. The analysis also considers the limitations of the period range covered by the MT data and how longer period GIC may be better calculated using the results of thin-sheet modelling of electric fields.

Two principal conclusions regarding GIC in the North Island can be drawn. Firstly, it is clear that magnetic field variations in the period range 2-30 minutes covered by the MT data result in significant GIC at several substations in the lower part of the North Island. Although the size of the calculated GIC resulting from the St. Patrick's Day Storm are not large in themselves, peak GIC in excess of 10A are commonly calculated for the 2003 storm. In the context of what might be expected during a major space weather event, such as has been estimated by Ingham et al. (2017) and Rodger et al. (2017), major disruption of the North Island transmission network could therefore be anticipated during extreme storms. Although the use of an equivalent circuit does not allow GIC calculation from the MT data for the northern part of the North Island network, calculation using uniform electric fields suggests that substations around Auckland, New Zealand's largest city, may also experience risk. Secondly, as seen in the analysis of THD by Rodger et al. (2020), and supported by GIC calculated from the thin-sheet model of Divett et al. (2107), it is apparent that longer period variations of the magnetic field are likely to result in significant GIC which may be sustained over long periods of time.

An implication of the limited period range of the MT data, and the potential ability of the thin-sheet model to better predict longer period GIC, is that improved broadband modelling of GIC might be achieved by combining the two techniques into a single prediction. Such an approach will be investigated in future work. It is also possible that, as an alternative to using an equivalent circuit, gaps in the MT data could be filled by using impedance tensor estimates calculated from the thin-sheet model. However, both of these approaches have a limitation in that the thin-sheet model is derived from 2 and 3-dimensional numerical models of resistivity structure based on MT data. As such any impedance tensor estimated from the thin-sheet model does not take into account galvanic distortions (e.g. static shift). Such distortions are almost invariably observed in the actual MT data, but are generally removed before modelling/inversion. Although removal of distortions is valid in terms of looking at regional structure, as most studies are designed to do, such distortions are real effects which do influence the production of GIC – a factor which is missing in relatively smooth thin-sheet conductance models.

Notwithstanding the above, the overall picture can probably best be refined both by targeting further MT measurements in the northern part of the North Island, and to fill in gaps in coverage further to the south, and by extending the period range of such measurements to longer periods. Nevertheless, the present results suggest that measurements of GIC, already prevalent in the South Island, should be extended to the North Island substations and transformers indicated in this study as being the most at risk.

Previous studies of GIC in New Zealand South Island have been based on thin-sheet modelling. The results presented here reinforce the point made by Divett et al. (2020) that such modelling tends to significantly underestimate GIC produced by rapid variations of the magnetic field. Nevertheless, thin-sheet conductance models provide a good first approximation to what can be expected in the generation of GIC. This in itself is useful to power network operators and probably sets a lower limit on what might be expected due to geomagnetic activity (potentially providing a lower but realistic estimate when modelling an "extreme" geomagnetic storm). Ideally, however, the same approach of using MT data in conjunction with the thin-sheet model to predict GIC in the South Island is desirable. This is particularly so given the wealth of GIC measurements on the South Island power network. Unfortunately, at present, in terms of the grid cells in the thin-sheet model, less than 10% contain MT sites and these are concentrated on three lines across the Island which are sufficiently well separated (by ~200-250 km) as to make interpolation of electric fields unreliable. Nonetheless, the possibility of modelling GIC using the equivalent circuit technique in association with the small number of MT sites in the far south of the South Island is being explored.

## Acknowledgments and Data

The work presented here was completed under the New Zealand Ministry of Business, Innovation and Employment Hazards and Infrastructure Research Fund Contract UOOX1502. Kamran Mukhtar was funded by a scholarship awarded under the same contract. The authors would like to thank Transpower New Zealand for supporting this study. The results presented in this paper rely on data collected at the EYR magnetic observatory downloaded from www.intermagnet.org . Transpower New Zealand collects GIC and THD observations as part of their commercial activity. Requests for access to GIC and THD observations should be addressed to Michael Dalzell (Michael.Dalzell@transpower.co.nz). The MT data used in this study were collected by Victoria University and GNS Science during numerous prior studies as referenced in the text. MT impedances measured by VUW may be downloaded from figshare.com at 10.6084/m9.figshare.12935192 .Requests for

access to data collected by GNS Science should in the first instance be addressed to Wiebke Heise (W.Heise@gns.cri.nz). The thin-sheet conductance model used in this paper and in other publications on GIC in New Zealand can be downloaded from 10.6084/m9.figshare.12935195.

## References

Bailey, R.L., T.S. Halbedl, I. Schattauer, A. Römer, G. Achleitner, C.D. Beggan, V. Wesztergom, R. Egli, & R. Leonhardt (2017). Modelling geomagnetically induced currents in midlatitude Central Europe using a thin-sheet approach. *Annales Geophysicae*, 35, 751–761, doi:10.5194/angeo-35-751-2017.

Bailey, R. L., T.S. Halbedl, I. Schattauer, G. Achleitner & R. Leonhardt (2018). Validating GIC models with measurements in Austria: Evaluation of accuracy and sensitivity to input parameters. *Space Weather*,16, 887–902, doi:10.1029/2018SW001842.

Beggan, C.D., D. Beamish, A. Richards, G.S. Kelly, G.S. & A.W. Thomson (2013). Prediction of extreme geomagnetically induced currents in the UK high-voltage network. *Space Weather*, 11, 407-419, doi:10.1002/swe.20065.

Bertrand, E.A., T.G. Caldwell, G.J. Hill, E.L. Wallin, S.L. Bennie, N. Cozens, S. A. Onacha, G.A. Ryan, C. Walter, A. Zaino, & P. Wameyo (2012). Magnetotelluric imaging of upper-crustal convection plumes beneath the Taupo Volcanic Zone, New Zealand. *Geophysical Research Letters*, 39 (2), 6, doi:10.1029/2011GL050177.

Bertrand, E.A., T.G. Caldwell, G.J. Hill, S.L. Bennie, & S. Soengkono (2013). Magnetotelluric imaging of the Ohaaki geothermal system, New Zealand: implications for locating basement permeability. *Journal of Volcanology and Geothermal Research*, 268, 36–45, doi:10.1016/j.jvolgeores.2013.10.010.

Blake, S.P., P.T. Gallagher, J. McCauley, A.G. Jones, C. Hogg, J. Campanya, C. Beggan, A.W.P. Thomson, G.S. Kelly & D. Bell (2016). Geomagnetically induced currents in the Irish power network during geomagnetic storms. *Space Weather*,14, 1136–1154, doi:10.1002/2016SW001534.

Bonner, L. R. & A. Schultz (2017). Rapid predictions of electric fields associated with geomagnetically induced currents in the presence of three-dimensional ground structure: Projection of remote magnetic observatory data through magnetotelluric impedance tensors. *Space Weather*, 15, 204–227, doi:10.1002/2016SW001535.

Boteler, D.H., A.J.C. Lackey, L. Marti, & S. Shelemy (2013). Equivalent circuits for modelling geomagnetically induced currents from a neighbouring network. Paper 002195 presented at IEEE Power & Energy Society GM, Vancouver, 21–25 July.

Boteler, D.H. & R. J. Pirjola (2014). Comparison of methods for modelling geomagnetically induced currents. *Annales Geophysicae*, *32*, 1177–1187, doi:10.5194/angeo-32-787 1177-2014.

Boteler, D.H. & R. J. Pirjola (2017). Modeling geomagnetically induced currents. *Space Weather*, 15, 258–276, doi:10.1002/2016SW001499.

Cassidy, J., M. Ingham, C.A. Locke, & H.M. Bibby (2009). Subsurface structure across the axis of the Tongariro Volcanic Centre, New Zealand. *Journal of Volcanology and Geothermal Research*, 179, 233–240, doi:10.1016/j.jvolgeores.2008.11.017.

Clilverd, M.A., C.J. Rodger, J.B.  Brundell, M. Dalzell, I. Martin, D.H. Mac Manus, D. H., N.R. Thomson, T. Petersen & Y.i Obana (2018). Long-lasting geomagnetically induced currents and harmonic distortion observed in New Zealand during the 7–8 September 2017 disturbed period. *Space Weather*, 16, 704–717. https://doi.org/ 10.1029/2018SW001822

Divett, T., M. Ingham, C.D. Beggan, G.S. Richardson, C.J. Rodger, A.W.P. Thomson & M. Dalzell (2017). Modeling geo-electric fields and geomagnetically induced currents (GIC) around New Zealand to explore GIC in the South Islands's electrical transmission network. *Space Weather*, 15, 1396-1412, doi:10.1002/2017SW001697.

Divett, T., G.S. Richardson, C.D. Beggan, C.J. Rodger, D.H. Boteler, M. Ingham, D.H. MacManus, A.W.P. Thomson & M. Dalzell (2018). Transformer-level modeling of geomagnetically induced currents in New Zealand's South Island. *Space Weather*, 16, 718-735, doi:10.1029/2018SW001814.

Divett, T., D.H. Mac Manus, G.S. Richardson, C.D. Beggan, C.J. Rodger, M. Ingham, E. Clarke, A.W.P. Thomson, M. Dalzell & Y. Obana (2020). Geomagnetically induced current model validation from New Zealand's South Island. *Space Weather*, doi: 10.1029/2020SW002494.

Girgis, R. S. & K.B. Vedante (2015). Impact of GICs on power transformers. IEEE Electrification Magazine.

Guillon, S., Toner, P., Gibson, L., & Boteler, D. (2016). A colorful blackout. *IEEE Power and Energy Magazine*, 14(6), 59–71, doi:10.1109/MPE.2016.2591760.

Heise, W., T.G. Caldwell, H.M. Bibby & S.C. Bannister (2008). Three-dimensional modelling of magnetotelluric data from the Rotokawa geothermal field, Taupo Volcanic Zone, New Zealand. *Geophysical Journal International*, 173 (2), 740–750, doi:10.1111/j.1365-246X.2008.03737.x.

Heise, W., T.G. Caldwell, H.M. Bibby & S.L. Bennie (2010), Three-dimensional electrical resistivity image of magma beneath an active continental rift, Taupo Volcanic Zone, New Zealand. *Geophysical Research Letters*, 37, L10301, doi:10.1029/2010GL043110.

Heise, W., T.G. Caldwell, G.J. Hill, S.L. Bennie, E. Wallin, & E.A. Bertrand (2012). Magnetotelluric imaging of fluid processes at the subduction interface of the Hikurangi Margin, New Zealand. *Geophysical Research Letters*, 39, L04308, doi:10.1029/2011GL050150.

Heise, W., E.A. Bertrand, T.G. Caldwell, G.J. Hill, N.. Palmer, & S.L. Bennie (2014). 2-D magnetotelluric imaging of the Rotorua and Waimangu geothermal fields. In Proceedings 36th New Zealand Geothermal Workshop, 24-26 November 2014, Auckland, New Zealand, p. 2, University of Auckland, Auckland, N.Z.

Ingham, M. (2005). Deep electrical structure of the Central Volcanic Region and Taupo Volcanic Zone, New Zealand, *Earth, Planets and Space*, 57 (7), 591–603, doi:10.1186/BF03351838.

Ingham, M., K. Whaler, & D. McKnight (2001). Magnetotelluric sounding of the Hikurangi Margin, New Zealand. *Geophysical Journal International*, 144 (2), 343–355, doi:10.1046/j.0956-540X.2000.01330.x.

Ingham, M.R., H.M. Bibby, W. Heise, K.A. Jones, P. Cairns, S. Dravitzki, S.L.Bennie, T.G. Caldwell, & Y. Ogawa (2009). A magnetotelluric study of Mount Ruapehu volcano, New Zealand. *Geophysical Journal International*, 179 (2), 887–904, doi:10.1111/j.1365-246X.2009.04317.x.

Ingham, M., C.J. Rodger, T. Divett, M. Dalzell, & T. Petersen, T., 2017Assessment of GIC based on transfer function analysis. Space Weather, 15, 1615-1627, doi:10.1002/2017SW001707.

Kappenman, J. G. (1996). Geomagnetic storms and their impact on power systems. IEEE Power Engineering Review, 16(5), 5.

Kelbert, A., C.C. Balch, A. Pulkkinen, G.D. Egbert, J.J. Love, E.J. Rigler, & I. Fujii (2017). Methodology for time-domain estimation of storm time geoelectric fields using the 3D magnetotelluric response tensors. *Space Weather*, 15, 874–894, doi: 10.1002/ 2017SW001594

Kelly, G. S., A. Viljanen, C. D. Beggan, & A. W. P. Thomson (2017). Understanding GIC in the UK and French high-voltage transmission systems during severe magnetic storms. *Space Weather*, 15, 99–114, doi:10.1002/2016SW001469

Lakhina, G.S. & B.T. Tsurutani (2016). Geomagnetic storms: historical perspective to modern view. *Geoscience Letters*, 3, 5, doi:10.1186/s40562-016-0037-4.

Lehtinen, M. & R. Pirjola (1985). Currents produced in earthed conductor networks by geomagnetically-induced electric fields. *Annales Geophysicae*, 3, 479-484.

Love, J. J., G.M. Lucas, A. Kelbert & P.A. Bedrosian (2018). Geoelectric hazard maps for the Mid-Atlantic United States: 100 year extreme values and the 1989 magnetic storm. *Geophysical Research Letters*, 45, 5–14, doi: 10.1002/2017GL076042.

Lucas, G. M., J.J. Love, & A. Kelbert (2018). Calculation of voltages in electric power transmission lines during historic geomagnetic storms: An investigation using realistic earth impedances. Space Weather, 16, 185–195, doi: 10.1002/2017SW001779.

Mac Manus, D.H., C.J. Rodger, M. Dalzell, A.W.P. Thomson, M.A. Clilverd, T. Petersen, M.M. Wolf, N.R. Thomson, & T. Divett (2017). Long term geomagnetically induced current observations from New Zealand: earth return corrections and comparison with geomagnetic field driver. *Space Weather*, 15, 1020-1038, doi:10.1002/2017SW001635.

McKay, A. J. (2003). Geoelectric fields and geomagnetically induced currents in the United Kingdom (PhD thesis), University of Edinburgh, https://era.ed.ac.uk/handle/1842/639.

McLoughlin, C., M. Ingham, K. Whaler, & D. McKnight (2002). A magnetotelluric transect of the Wairarapa region, New Zealand. *New Zealand Journal of Geology and Geophysics*, 45, 257–269, doi:10.1080/00288306.2002.9514972.

Navia, C.E., Marcel N. de Oliveira & Carlos R.A. Augusto (2018). The Highest Geomagnetic Storms of the Solar Cycle Observed at Ground Level, in *Extreme Weather*, ed: Philip John Sallis, IntechOpen, doi: 10.5772/intechopen.75688.

Rodger, C.J., D.H. Mac Manus, M. Dalzell, A.W.P. Thomson, E. Clarke, T. Petersen, M.A. Clilverd, & T. Divett (2017). Long-Term geomagnetically induced current observations from New Zealand: peak current estimates for extreme geomagnetic storms, *Space Weather*, 15, 1447–1460, doi:10.1002/2017SW001691.

Rodger, C.J., M.A. Clilverd, D.H. Mac Manus, I. Martin, M. Dalzell, J.B. Brundell, T. Divett & N.R. Thomson (2020). Geomagnetically Induced Currents and Harmonic Distortion: Storm-time Observations from New Zealand. *Space Weather*, doi:10.1029/2019SW002387.

Stagpoole, V., S. Bennie, H. Bibby, S. Dravitzki, & M. Ingham (2009). Deep structure of a major subduction back thrust: Magneto-telluric investigations of the Taranaki Fault, New Zealand. *Tectonophysics*, 463, 77–85, doi:10.1016/j.tecto.2008.09.035.

Torta, J.M., A. Marcuello, J. Campanyà, S. Marsal, P. Queralt & J. Ledo (2017). Improving the modeling of geomagnetically induced currents in Spain. *Space Weather, 15*, 691-703, doi: 10.1002/2017SW001628.

United Nations Committee on the Peaceful Uses of Outer Space Expert Group on Space Weather (2017), Report on Thematic Priority 4: International Framework for Space Weather Services for UNISPACE+50 (A/AC.105/1171).

Vasseur, G. & P. Weidelt (1977), Bimodal electromagnetic induction in non-uniform thin sheets with an application to the northern Pyrenean induction anomaly. *Geophysical Journal International*, 51 (3), 669–690, doi:10.1111/j.1365-246X.1977.tb04213.x.

## Figure Captions

Figure 1: Outline map of New Zealand showing locations mentioned in the text.

Figure 2: Variations in the horizontal magnetic field components at EYR geomagnetic observatory during (a) the St. Patrick's Day Storm of 2015, (b) the storm of 20 November 2003.

Figure 3: Example of electric fields during the St. Patrick's Day storm at site MTR106 calculated using interpolation of the MT impedance tensor in the period range 2-30 minutes.

Figure 4: The North Island part of the thin-sheet conductance model used by Divett et al. (2017). Model cells containing MT sites are marked by black dots. The white dot marks the location of site MTR106.

Figure 5: The North Island transmission network. As discussed in the text, the region to the north-west of the black dashed line has been represented by an equivalent circuit for GIC calculation.

Figure 6: Comparison of the results of the interpolation/extrapolation of electric fields derived from MT data by two different techniques, for two instants of time during the 2015 St. Patrick's Day storm. Actual fields at MT sites calculated from the impedance data are shown by white arrows.

Figure 7: Comparison of the results of calculation of GIC using a uniform electric field of 1 V/m, in the orientation indicated by the arrow, for both the entire North Island network (red) and using the equivalent circuit approach described in the text (blue).

Figure 8: Substation-level calculated GIC at New Plymouth (NPL) for (a) the St. Patrick's Day 2015 storm and (b) the 20 November 2003 storm. GIC calculated from the MT data are shown in black. GIC calculated from the thin-sheet model are shown in red. GIC calculated from the thin-sheet model have been band-pass filtered to match the frequency range of the MT data.

Figure 9: GIC in the lower North Island calculated from MT electric fields for 18:48 UT on 20 November 2003.

Figure 10: Unfiltered substation-level GIC at New Plymouth (NPL) calculated from the thin-sheet model. Also shown is the variation in $B_x$ at EYR during the St. Patrick's Day Storm.

Figure 11: (a) GIC in transformer T8 at NPL calculated from MT measurements during the 2-hour period from 17:30 to 19:30 on 20/11/2003. (b) Unfiltered GIC during the 20 November 2003 storm calculated from the thin-sheet model.

Figure 12: (a) South Island transmission network showing connections to Islington substation. (b) Locations of Islington (ISL) and Redclyffe (RDF) relative to the conductance map of New Zealand. (c) Comparison of MT calculated GIC at RDF T1 and observed GIC at ISL T6 around the sudden storm commencement of the St. Patrick's Day 2015 storm.

Figure 13: Rates of change of $B_x$ at an MT site close to New Plymouth plotted against the same as observed at the geomagnetic observatory at Eyrewell for the period 0539-1039 UT 11 November 2019.

## Tables

| Line | Substation node (From) | Substation node (To) | Resistance (Ω) | Line length (km) |
|---|---|---|---|---|
| 1 | ARI110_2 | BOB110_1 | 8.20 | 122.02 |
| 2 | ARI110_2 | HAM110_1 | 3.28 | 47.00 |
| 3 | ARI110_2 | HAM110_1 | 3.28 | 46.56 |
| 4 | WKM220_1 | OTA220_1 | 5.37 | 190.78 |
| 5 | WKM220_1 | OTA220_1 | 5.37 | 190.89 |
| 6 | WKM220_2 | BHL220_1 | 0.86 | 185.19 |
| 7 | WKM220_2 | BHL220_2 | 0.86 | 185.19 |
| 8 | WKM220_1 | HAM220_1 | 0.411 | 90.93 |
| 9 | WKM220_1 | OHW220_2 | 0.53 | 118.42 |
| 10 | TMN220_1 | TWH220_1 | 0.33 | 144.93 |
| 11 | SFD220_1 | HLY220_1 | 0.64 | 280.49 |

Table 1: Transmission lines, connecting southern and northern parts of the North Island network, which have been earthed at the northern end in the calculation of GIC.

| | NPL (MT) | NPL (thin-sheet) | RDF (MT) | RDF (thin-sheet) |
|---|---|---|---|---|
| **0950-1000** | 1.0 A | 3.3 A | 1.2 A | 2.3 A |
| **1320-1330** | 1.3 A | 1.5 A | 1.6 A | 2.1 A |

Table 2: 10-minute averaged values of GIC magnitude at New Plymouth (NPL) and Redclyffe (RDF) for two periods during the St. Patrick's Day storm calculated from MT data and from the thin-sheet model.

**Figure 1.**

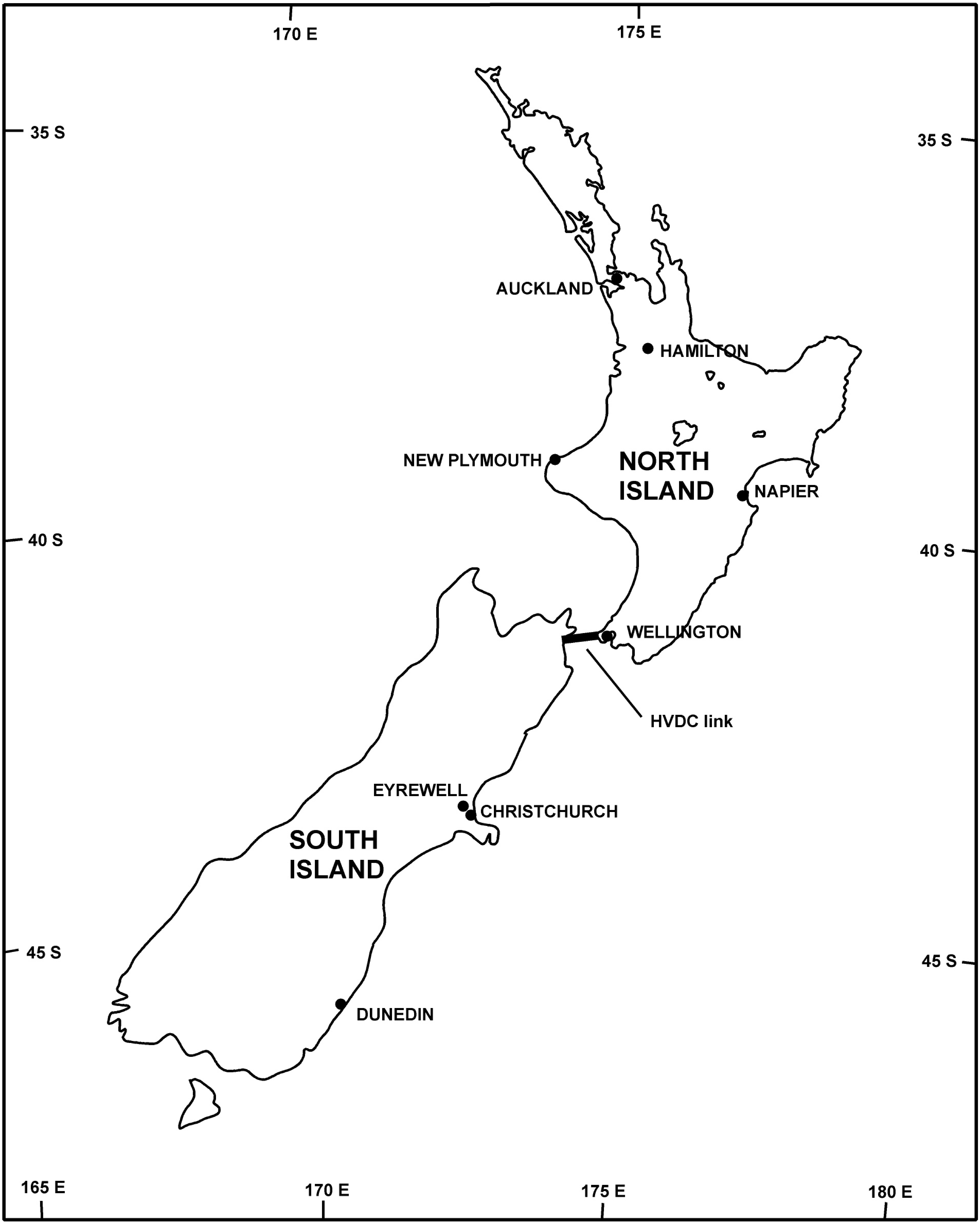
170 E
175 E
35 S
35 S
AUCKLAND
HAMILTON
NEW PLYMOUTH
NORTH ISLAND
NAPIER
40 S
40 S
WELLINGTON
HVDC link
EYREWELL
CHRISTCHURCH
SOUTH ISLAND
45 S
45 S
DUNEDIN
165 E
170 E
175 E
180 E

**Figure 2.**


Bx (nT)
19500
19400
19300
19200
19100
19000
0:00
6:00
12:00
18:00
0:00
6:00
By (nT)
8400
8300
8200
8100
8000
(a)
0:00
6:00
12:00
18:00
0:00
6:00
Time from 0:00 17/03/2015 UT
Bx (nT)
19600
19200
18800
18400
18000
6:00
12:00
18:00
0:00
6:00
12:00
By (nT)
8400
8200
8000
7800
(b)
6:00
12:00
18:00
0:00
6:00
12:00
Time from 06:00 20/11/2003 UT

**Figure 3.**

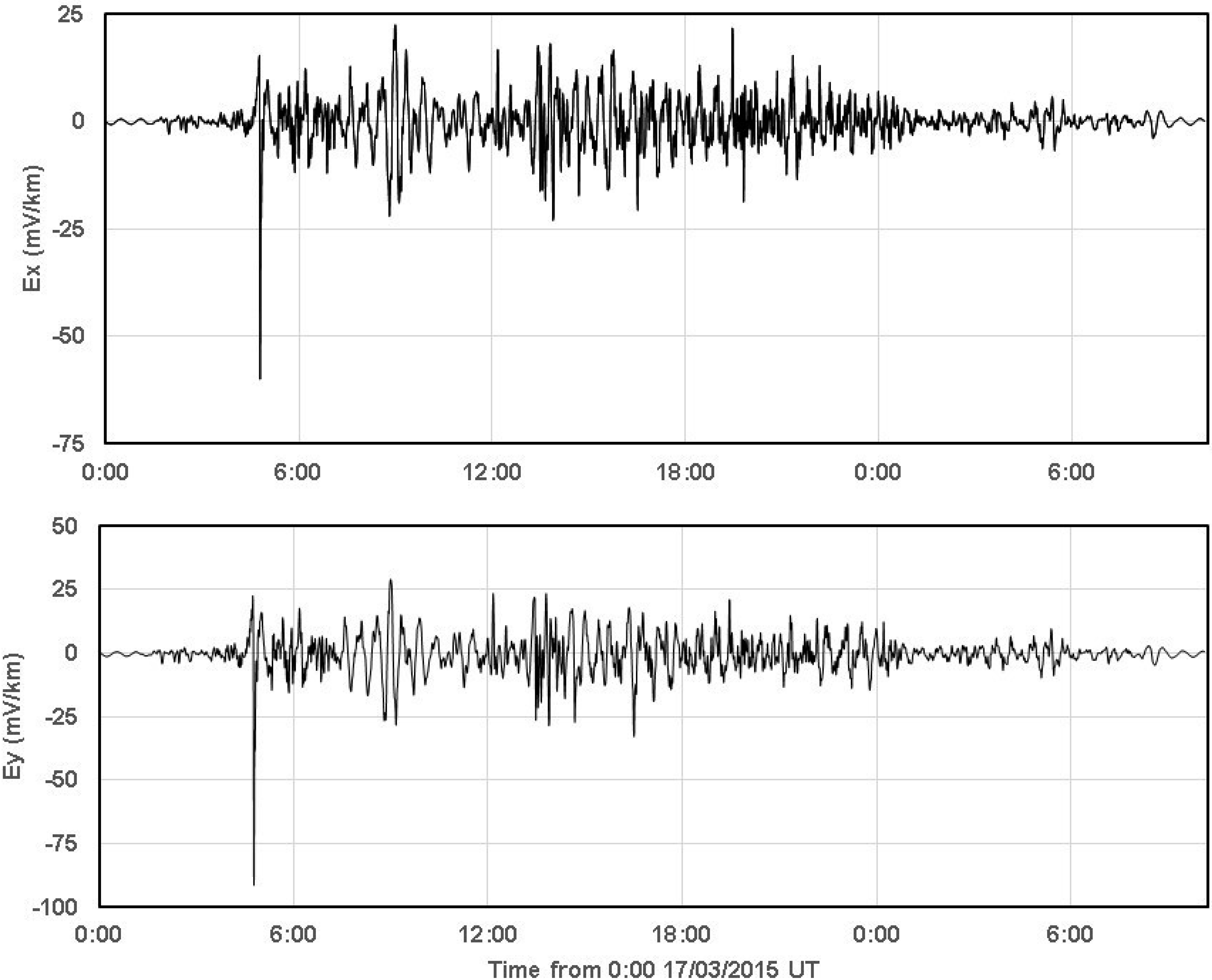

25
0
-25
-50
-75
Ex (mV/km)
0:00
6:00
12:00
18:00
0:00
6:00
50
25
0
-25
-50
-75
-100
Ey (mV/km)
0:00
6:00
12:00
18:00
0:00
6:00
Time from 0:00 17/03/2015 UT

**Figure 4.**

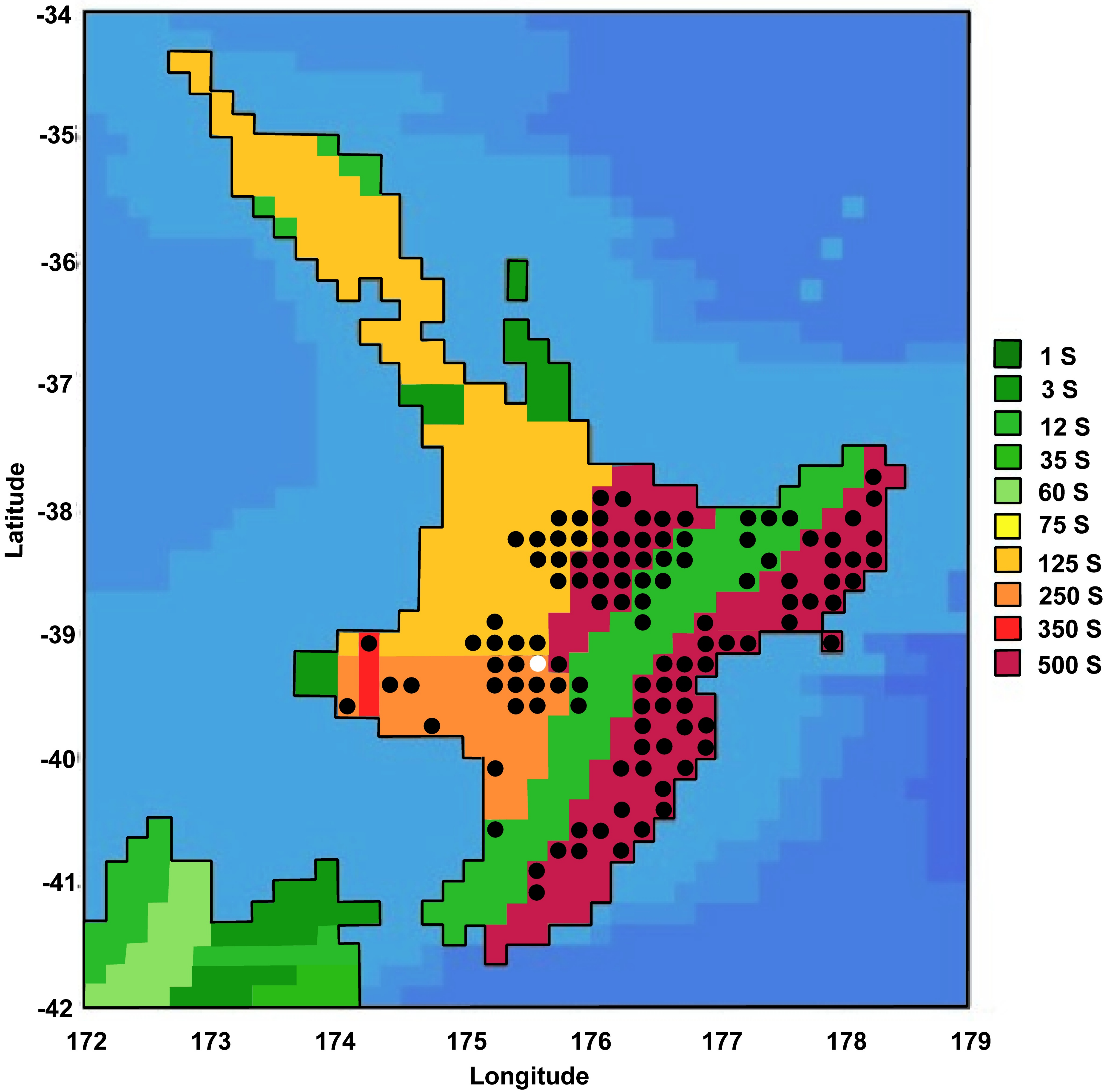

-34
-35
-36
-37
-38
-39
-40
-41
-42
Latitude
172
173
174
175
176
177
178
179
Longitude
1 S
3 S
12 S
35 S
60 S
75 S
125 S
250 S
350 S
500 S

**Figure 5.**


PEN
OTA
BHL
BOB
OHW
HLY
TWH
HAM
ARI
KAW
AMU
WKM
TMN
NPL
SFD
RDF
BPE
HAY
400 kV
220 kV
110 kV
Power stations
Substations

**Figure 6.**

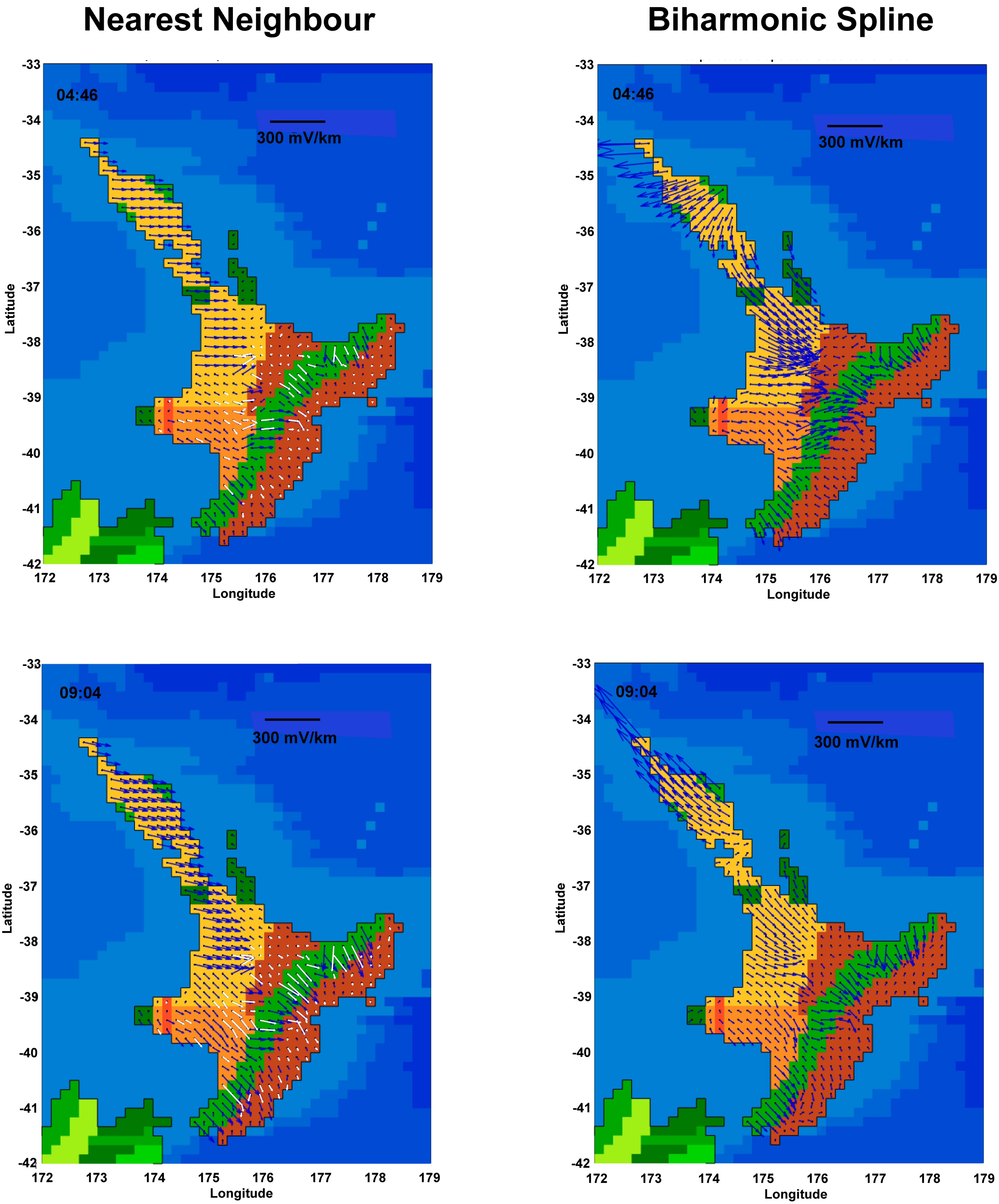

Nearest Neighbour
Biharmonic Spline
04:46
300 mV/km
09:04
300 mV/km
Latitude
Longitude
-33
-34
-35
-36
-37
-38
-39
-40
-41
-42
172
173
174
175
176
177
178
179

**Figure 7.**

GIC (A)
Full network
Equivalent circuit
KWA
WIL
HAY
BPE
RDF
WHI
SFD
RPO
NPL
TKU
MNI
TUI
PPI
WRK
ARA
OKI
WKM
OHK
ATI
MTI
WPA
KIN
MAT
LFD
KAW
TRK
ARI
WAI
EDG
KPO

**Figure 8.**

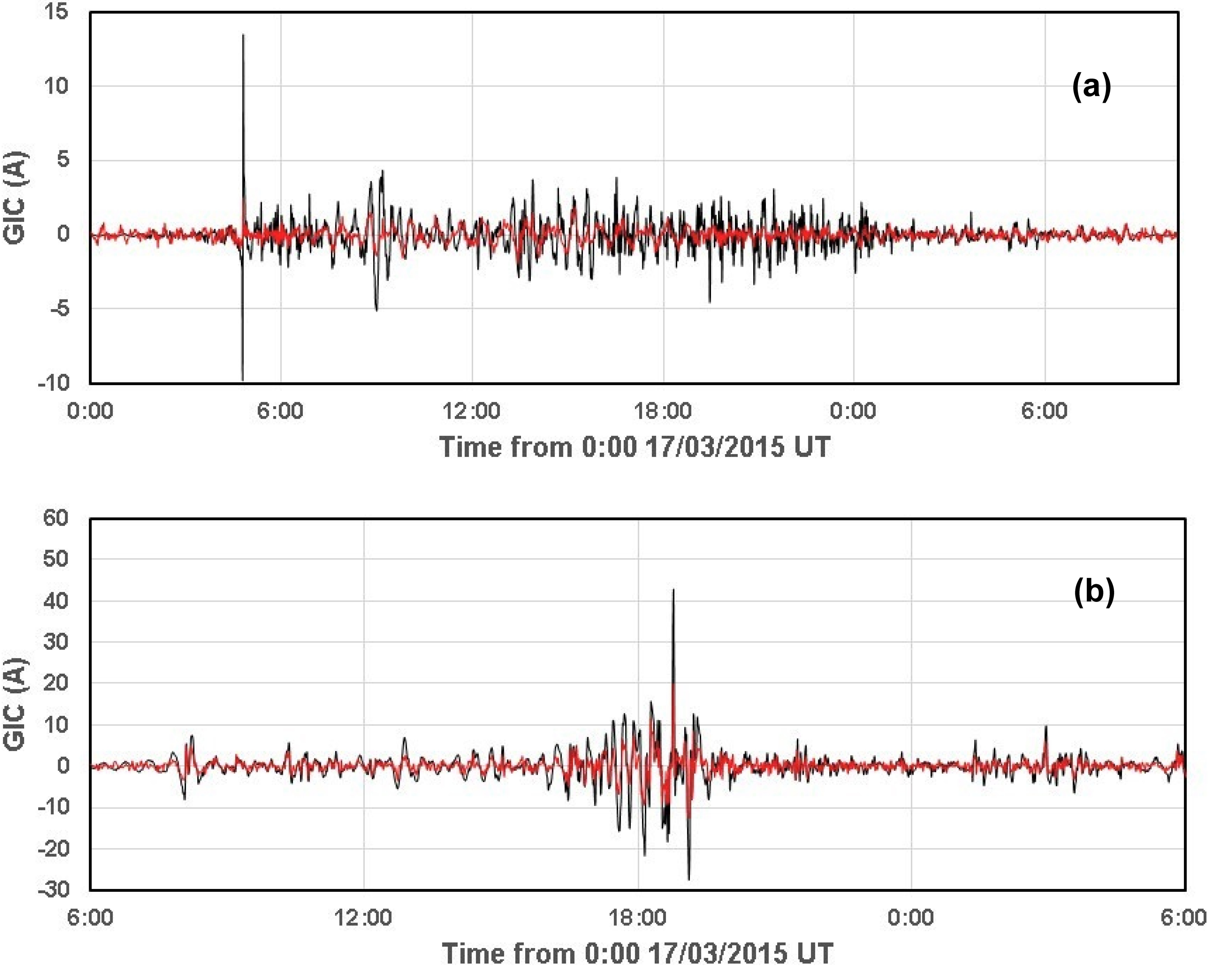

(a)
15
10
5
0
-5
-10
GIC (A)
0:00
6:00
12:00
18:00
0:00
6:00
Time from 0:00 17/03/2015 UT
(b)
60
50
40
30
20
10
0
-10
-20
-30
GIC (A)
6:00
12:00
18:00
0:00
6:00
Time from 0:00 17/03/2015 UT

**Figure 9.**


KPO
EDG
WAI
ARI
TRK
KAW
LFD
MAT
KIN
WPA
MTI
ATI
OHK
WKM
OKI
ARA
WRK
PPI
TUI
MNI
TKU
NPL
RPO
SFD
WHI
RDF
BPE
HAY
WIL
KWA
-20
-10
0
10
20
30
40
50
GIC (A)

**Figure 10.**

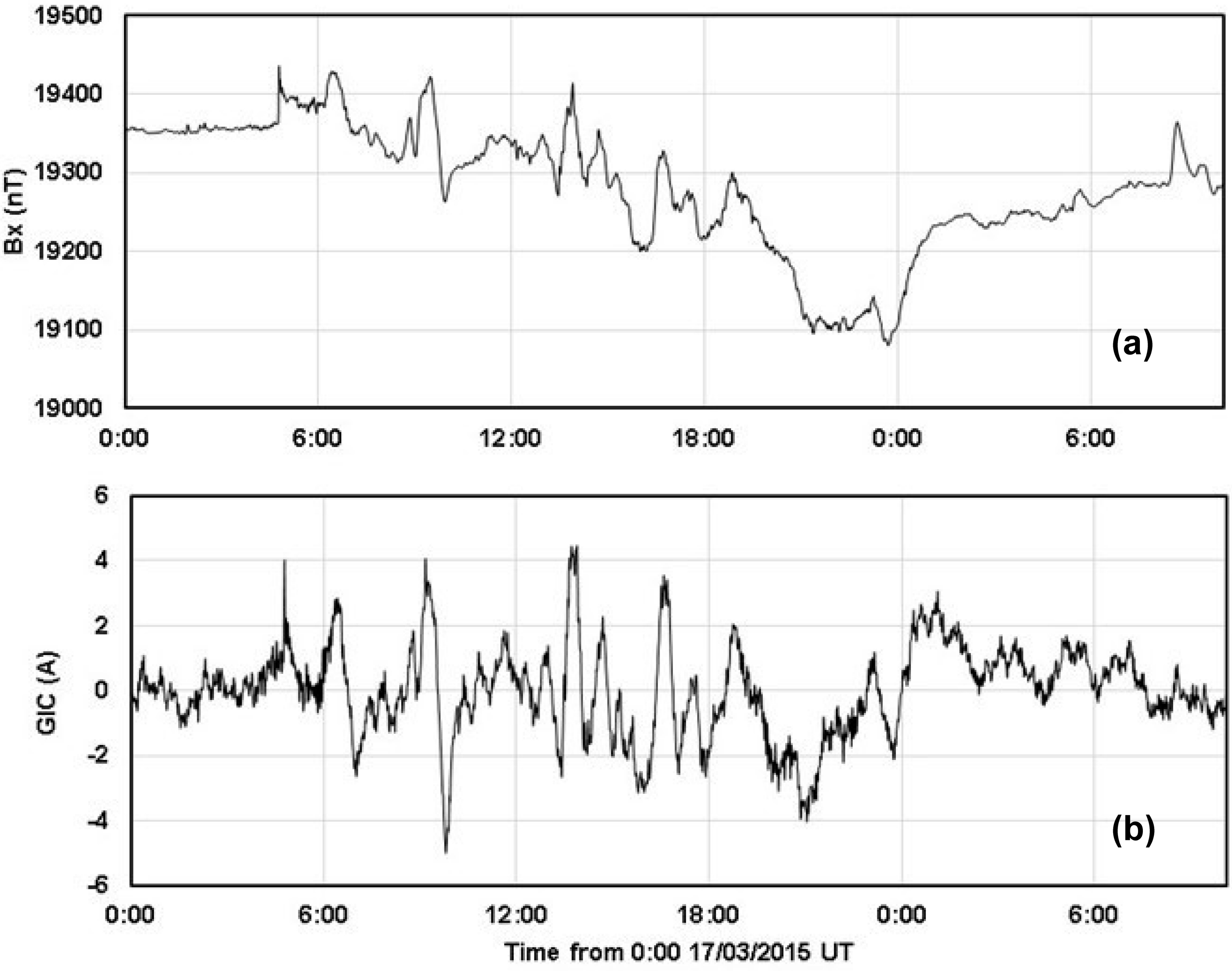
19500
19400
19300
19200
19100
19000
Bx (nT)
(a)
0:00
6:00
12:00
18:00
0:00
6:00
6
4
2
0
-2
-4
-6
GIC (A)
(b)
0:00
6:00
12:00
18:00
0:00
6:00
Time from 0:00 17/03/2015 UT

**Figure 11.**

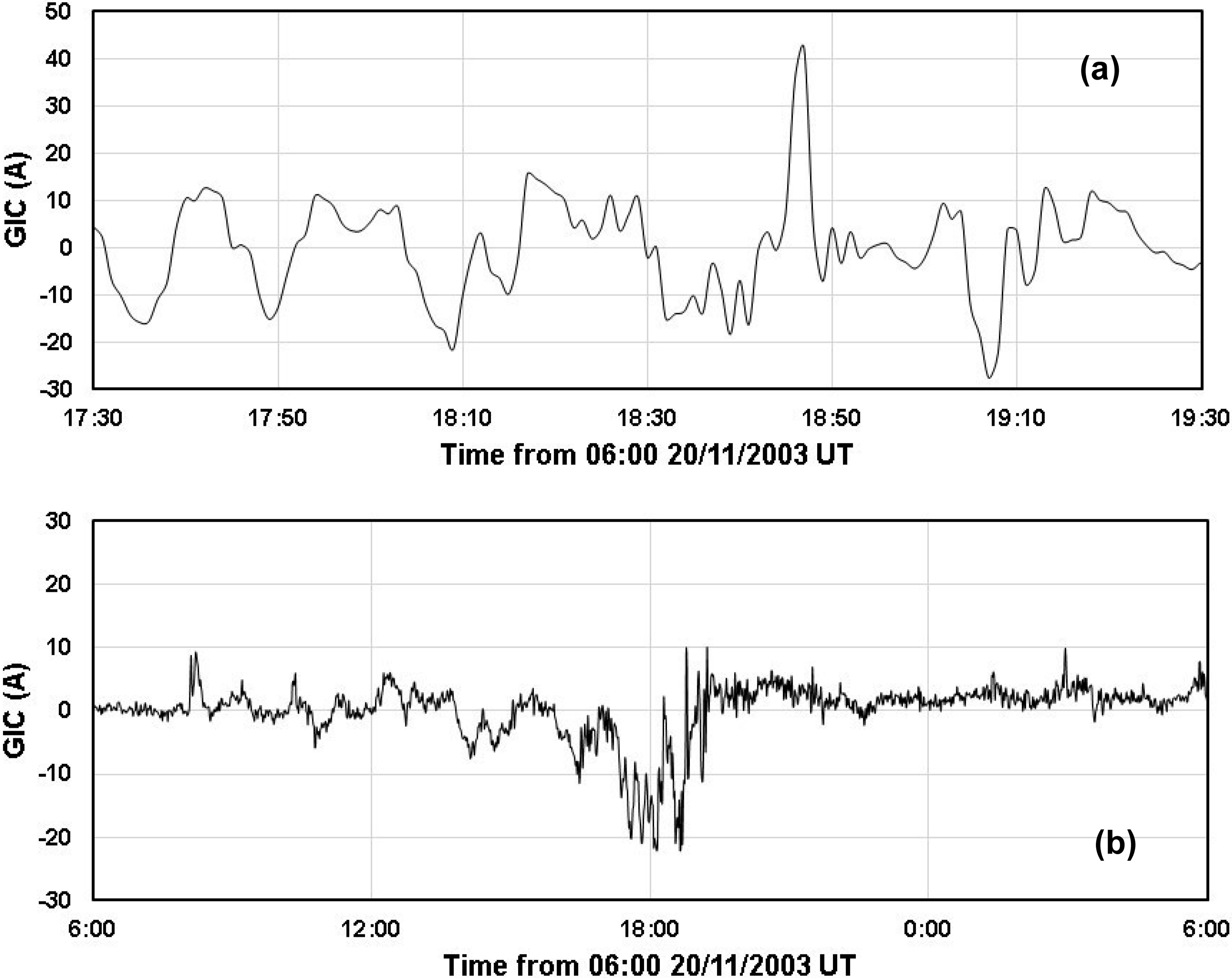

(a)
GIC (A)
50
40
30
20
10
0
-10
-20
-30
17:30
17:50
18:10
18:30
18:50
19:10
19:30
Time from 06:00 20/11/2003 UT
(b)
GIC (A)
30
20
10
0
-10
-20
-30
6:00
12:00
18:00
0:00
6:00
Time from 06:00 20/11/2003 UT

Figure 12.

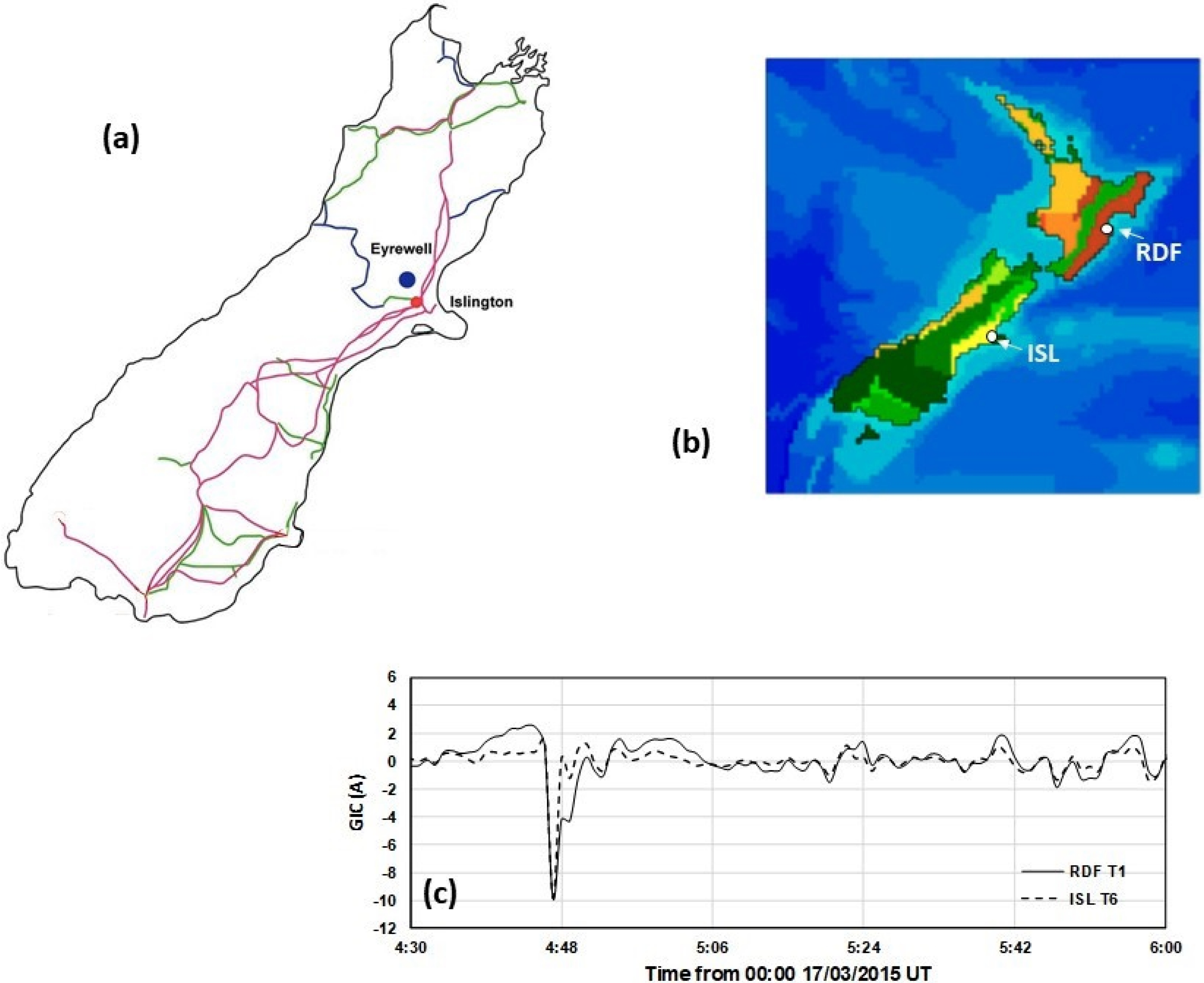
(a)
Eyrewell
Islington
(b)
RDF
ISL
(c)
GIC (A)
6
4
2
0
-2
-4
-6
-8
-10
-12
4:30
4:48
5:06
5:24
5:42
6:00
Time from 00:00 17/03/2015 UT
RDF T1
ISL T6

**Figure 13.**

8
6
4
2
0
-2
-4
-6
-8
dBx/dt (NPL)
-8
-6
-4
-2
0
2
4
6
8
dBx/dt (EYR)